Theme: Marine Ecosystem Characterization

Case Study 14

Biological Response Associated With a Coastal Upwelling Event

Hervé Demarcq*[1], Dominique Dagorne[2] and Jacobus J. Agenbag[3]

14.1 Introduction and Background

This case study deals with one of the most powerful coastal upwelling regions on Earth. Upwelling is a physical phenomenon that sustains very high levels of marine life and diversity. The area of interest is the southern part of the Benguela upwelling region, particularly the west coast of Southern Africa, from 28 to 34°S. The Lüderitz upwelling cell, situated a little further north (at 27.5°S), where the trade winds blow strongly all year round, is one of the largest upwelling cells in the world, making this area a quasi-physical barrier, even for some small pelagic fish populations. At this location, the wind speed is very high (always >5 m s^{-1}) and the high turbulence level, associated with a relatively low water clarity and a strong offshore component of the currents, makes this particular area relatively unfavourable for the survival of ichthyoplankton (eggs and fish larvae) compared with the rest of the system, where the upwelling is less intense.

NASA's MODIS (Moderate Resolution Imaging Spectroradiometer) sensor, on board the Terra and Aqua polar orbiting satellites, offers a unique opportunity to study physical and bio-chemical processes occurring near the sea surface, by providing simultaneous views of both sea surface temperature (SST) and ocean colour (most common product is chlorophyll-*a* concentration). We use simultaneous synoptic views of SST and surface chlorophyll-*a* concentration (SCC) to describe and interpret the main spatio-temporal processes that occur in this highly dynamic coastal area. More precisely, the goal of this case study is to use spatially explicit, instantaneous information from both variables to explore the enrichment mechanisms that occur in the euphotic layer (i.e. the layer of the sea surface illuminated by sun light where photosynthesis can take place), in terms of mesoscale activity

[1]Institut de Recherche pour le Développement, Avenue Jean Monnet, BP 171, 34203 Sète cedex, France. **Email address:* demarcq@ird.fr

[2]Institut de Recherche pour le Développement, Centre de Bretagne - BP 70, 29280 - Plouzané, France

[3]Marine and Coastal Management, Department of Environmental Affairs and Tourism, Private Bag X2, Rogge Bay 8012, South Africa

and algal growth. The availability of both SST and SSC from the same satellite is of crucial importance to understanding the links between the physics and the biology, and therefore to estimate the dynamics of the next trophic level, composed of zooplankton and ichthyoplankton that are highly sensitive to the environmental forcing that contributes to their survival, and ultimately to the success of their recruitment. Consequently pelagic fish species have developed specific strategies that take advantage of the richness of this region while minimizing the impact of the high environmental variability.

14.2 Materials and Methods

14.2.1 Information about image data

SST and ocean-colour data was acquired by the MODIS sensor on board the Aqua platform. MODIS data is disseminated via NASA's Ocean Color web site (`http://oceancolor.gsfc.nasa.gov/`) from where the SST and chlorophyll-*a* data for this case study can be downloaded. These data can be processed using the dedicated SeaDAS software freely available at `http://oceancolor.gsfc.nasa.gov/seadas/`. MODIS detects emitted and reflected radiance in 36 channels spanning the visible to infrared (IR) spectrum. Further information about the instrument can be found on the NASA MODIS web site at `http://modis.gsfc.nasa.gov/about/specifications.php`. The standard MODIS Chlorophyll-*a* algorithm (OC3; O'Reilly et al., 2000) relies on reflectance ratios at channels at 443, 488 and 551 nm.

The SST data used in this case study originates from the infrared part of the spectrum, between 11 and 12 μm. A second SST measurement (not used here) is also recorded at three wavelengths between 3.7 and 4.0 μm in the near infrared part of the spectrum. The electromagnetic radiation emitted from the sea surface can be inverted (using Planck's law, see `http://en.wikipedia.org/wiki/Planck's_law`) to deduce the surface temperature of the target. For remote sensing applications, the 11–12 μm spectral window is used most frequently because of its relatively low sensibility to the Earth's atmosphere. The nominal image resolution of the data (at the satellite nadir) is 1 km and its effective radiometric resolution for SST is 0.1°C. The chlorophyll concentration is displayed using a chlorophyll scale with values ranging from 0.01 to 58 mg chl-*a* m^{-3}. Both parameters are extracted from "Level 2" data i.e. in orbit form, including geolocation and atmospheric correction.

Wind data from the SeaWinds scatterometer, on board the QuikSCAT satellite, was also used in this case study. QuikSCAT was launched in June 1999 after the unexpected failure of the NASA scatterometer (NSCAT) satellite. The SeaWinds instrument is a specialized microwave radar that measures both the speed and direction of winds at the sea surface, at a spatial resolution of 25 km. This mission ended operation on 21 November 2009 due to an antenna rotation failure. The wind data used in this study are "Level 3" i.e. gridded and spatially and temporally combined.

14.2.2 Description of physical processes

The coastal upwelling principle was determined by physicist W.K. Ekman (1905) who examined the frictional effects of wind moving over the ocean surface. The net effect is that the current flow induced by the wind friction is deviated to the right of the wind direction in the northern hemisphere, and to the left of the wind direction in the southern hemisphere (Figure 14.1a). At the surface, the current moves at an angle of about 45 degrees to the wind direction. The net transport of water through the entire wind-driven water column is approximately 90 degrees to the direction of the wind. This movement of water is called **Ekman transport** or **Ekman flow**. Figure 14.1b shows the simplified cross-shore section of the water flow.

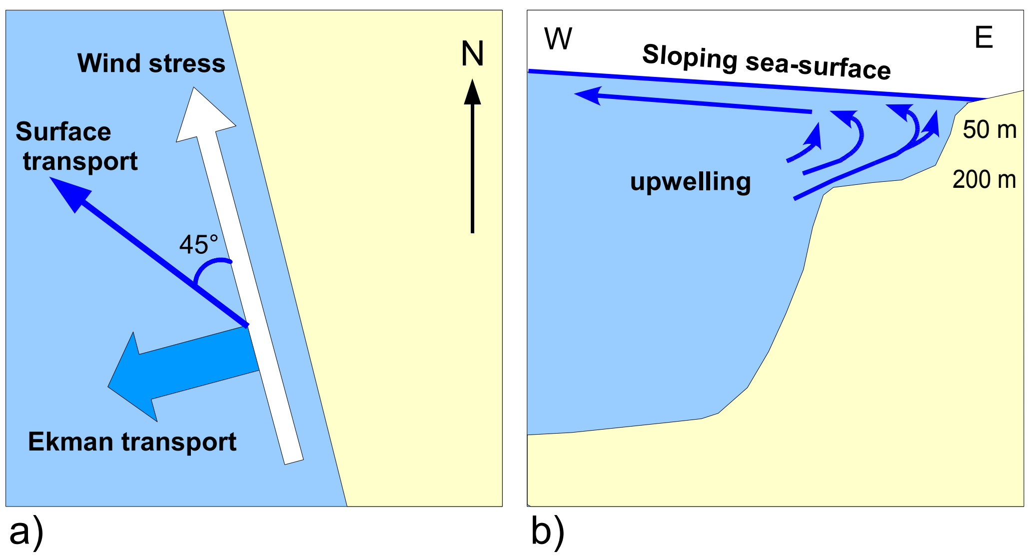

Figure 14.1 Schematic illustration of wind-driven, coastal upwelling in the southern hemisphere due to Ekman transport (adapted from Ocean Circulation, by The Open University).

Winds and currents thus combine to bring cold water from below the seasonal thermocline (50-200 m) to the surface, especially near the coast where the upwelling flow is maximum. Because of the temperature difference between the the coastal and offshore water masses, the surface temperature is a very good descriptor of coastal upwelling (Figure 14.2a), the dynamics of which can be studied from space. Furthermore, ocean-atmosphere interactions make these regions less cloudy than many other coastal regions. The presence of cold surface water decreases the evaporation, and therefore lowers the water vapor content of the atmosphere (one of the major absorbing components of the remote sensing reflectance signal, together with clouds and aerosols). Figure 14.2a shows that the coldest water (in white) is very close to the coast, a primary physical characteristic of a coastal upwelling region, and the most visible from space. Figure 14.2b shows the corresponding concentration of chlorophyll-*a* (the main photosynthetic pigment of most unicellular algae). The comparison between the SST and SCC images shows that, at first glance, there is a strong spatial link between both parameters. The mechanisms responsible for this relationship are the focus of this case study.

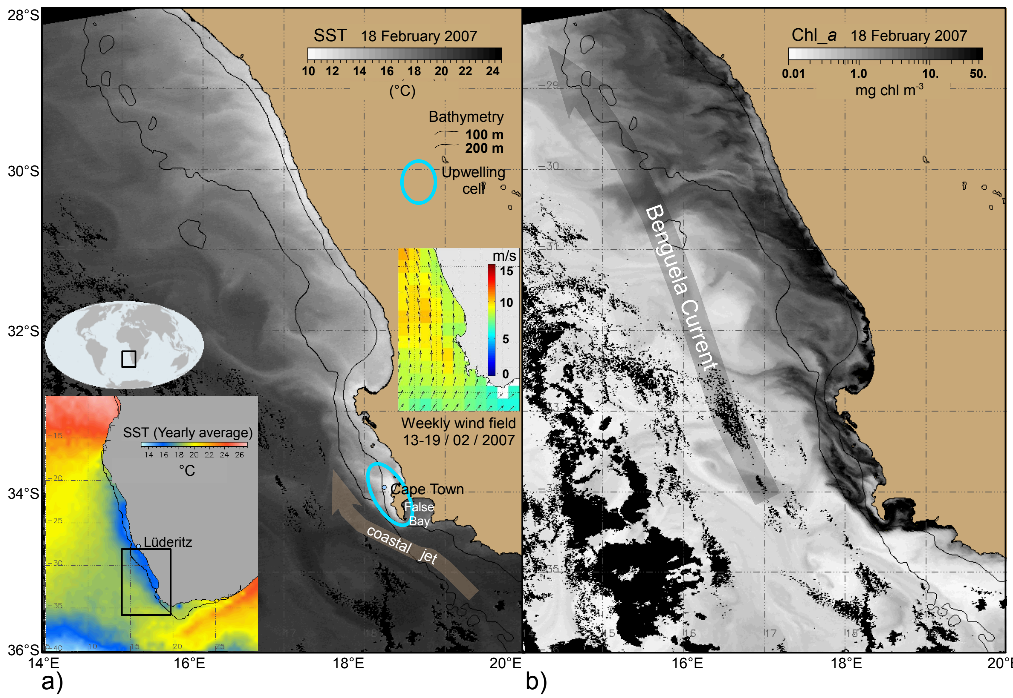

Figure 14.2 Region of interest showing (a) SST (°C) and (b) chlorophyll-a concentration (mg m^{-3}) computed from MODIS satellite data for the southern Benguela upwelling system, on 18 February 2007, during the upwelling season. The spatial resolution is 1 km. The left colour insert is the yearly average SST for the whole Benguela region, and the right insert is the average wind field during the week preceding the MODIS observation. The black patches in the offshore part of the chlorophyll image are due to lack of data because of the presence of clouds. MODIS data provided by NASA/GSFC.

Satellite images provide a synoptic view that allows a precise description of the spatial extent of the superficial upwelled waters. More precisely, the SST difference between the coastal and the offshore water allows a semi-quantification of the upwelling intensity based on the surface cooling. Such differences have been used to compute a SST-based coastal upwelling index (see Demarcq and Faure, 2000). The intensity of the coastal cooling is not homogeneous along the coast, but is reinforced in some locations where the vertical surface flux is stronger. These areas are called upwelling "cells". One in particular is clearly visible at the southern part of the region, between Cape Town and the Cape of Good Hope, the southwestern tip of the Cape Peninsula.

Fronts, eddies, plumes and filaments are the main signatures of mesoscale activity at the sea surface, and are primarily visible from satellite SST images because the water masses involved in frontogenesis (the formation or strengthening of a front) are generally of different temperatures. These features can also be observed through the "colour" of the sea, from maps of surface Chlorophyll-*a* concentration, the most widely used ocean colour product. In coastal upwelling areas, fronts and filaments are useful tracers of marine productivity and of the retention processes associated with the coastal circulation of water masses. Retention processes allow eggs and larvae of many pelagic species (or demersal and benthic species which have a pelagic early life stage) to be retained in favourable coastal areas, instead of being advected offshore.

Bakun's triade hypothesis (Bakun, 2006) provides a conceptual scheme for this mechanism. Bakun proposed that biological success is only possible in a marine environment if a satisfying balance is preserved between three fundamental physical processes: enrichment, concentration and retention. In coastal areas, enrichment processes are represented by the nutrient-rich, upwelled waters that enter the euphotic zone. The "concentration" term represents the vertical and horizontal advection of water masses that result in the concentration of biological matter, primarily phytoplankton. Last, but not least, the retention processes represents the ability of surface currents to keep the planktonic portion of the marine life (phytoplankton, zooplankton and ichthyoplankton) in particular areas where they will be more protected from predators and/or unfavourable environmental conditions. Marine species that have evolved in such a variable environment, have developed strategies that minimize the negative impacts while maximizing the favourable ones. For example, anchovies in the study region have developed a strategy to spawn in warmer waters (the extreme southern part of the system) which are physiologically more adequate for spawning. The eggs and larvae then drift away, pushed westward (but maintained close to the coast) by the coastal jet, where they are then passively transported to favourable retention areas where food is abundant. Naturally, over 90% of the released eggs are lost, but the survival of the species is preserved. Upwelled waters have high nutrient concentrations as a result of the sinking of organic matter (decaying phytoplankton blooms) from the sunlit surface layers into the deep ocean, where the cells are decomposed by bacteria. This process enriches the deep waters with nutrients (mainly nitrate, silicate and phosphate) which cannot be used at depth because the light levels are too low for photosynthesis.

Biologically, the newly upwelled water becomes progressively richer in chlorophyll and the maximum phytoplanktonic growth is reached when the uptake of nutrients becomes a limiting factor. The spatial heterogeneity of the surface currents, due to the complexity of the bathymetry combined with the heterogeneity of the wind field, creates mesoscale structures, visible on both the temperature and chlorophyll fields (Figure 14.2a,b). The intensity of these surface currents, as well as their induced retention effect on passive particles (or inversely their dispersal effect) are of primary importance in fisheries biology because they can cause the ichthyoplankton to drift far away from the coast where the feeding conditions are much less favourable for their survival. Consequently, the recruitment of these species could be impacted strongly by the natural variability of these currents. For example, it has been shown from satellite imagery that the length of the "pathway" associated with the meanders of the coastal jet in the southern Cape (Figure 14.2a), where both SST and chlorophyll gradients are very strong, is positively related to larvae survival, and therefore to the recruitment of the anchovy populations (Van der Lingen, 2006).

Note about colour palettes: The main images in Figure 14.2 are displayed in gray scale, the most objective way to represent a spatial continuum of a two-dimensional field for a single geophysical parameter. The disadvantage of a colour scale is the risk of artificially "contrasting" some parts of the image because a colour scale is always a compromise between smooth colour changes and a continuous light gradient. In a gray scale image, the light gradient is perfect and the eye is not influenced by the brightness of some colours. This is the best way to evaluate the global gradient of the image values. On the other hand, the determination of the local values is not as precise as for a colour scale (which is better in this respect), but far less objective for gradient estimation. Figures 14.3 and 14.4 show these two images using a false colour palette.

14.3 Training and Questions

Q1: Considering the physical principle of coastal upwelling (see Figure 14.1), how could it be characterized from a thermal point of view? What is the thermal contrast with the offshore oceanic water?

Q2: What mesoscale structures are visible in the SST and Chlorophyll images, either related to coastal upwelling processes, or not?

Q3: What is the main relationship between SST and SCC in the study area? In particular, how can you interpret the spatial information in terms of temporal history?

Q4: What are the main characteristics of the upwelling cells from the information available in the images, and what explanations can you give compared to the rest of the upwelling area?

Q5: What could be a suitable place for fish larvae to feed and survive in reasonably good conditions, with a low probability of being driven offshore where the predation pressure is higher? Look at the direction of the currents and topographic

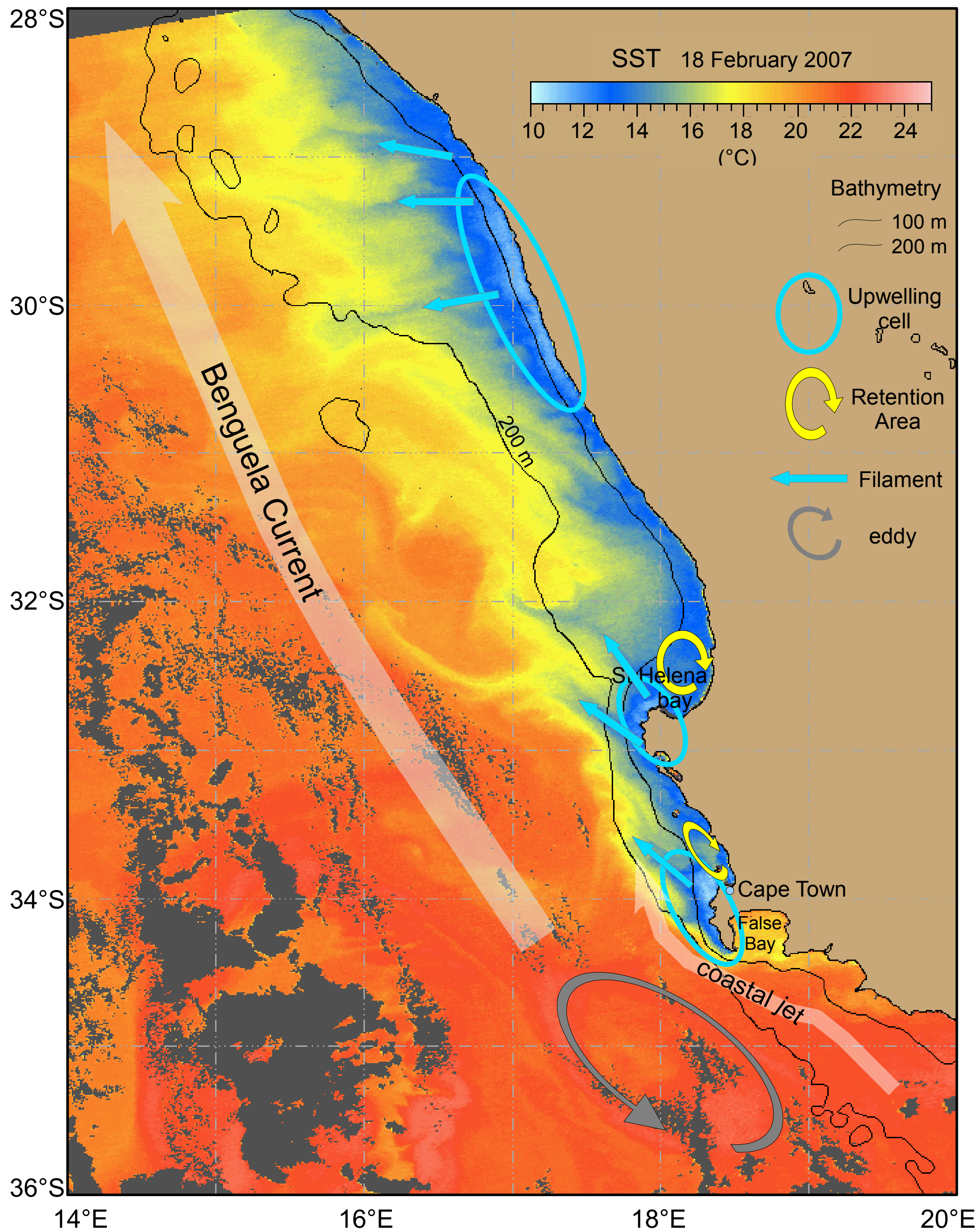

Figure 14.3 Same as Figure 14.2a (SST) but using a colour palette. Upwelling cells, associated filaments and retention areas are superimposed. MODIS data provided by NASA/GSFC.

opportunities.

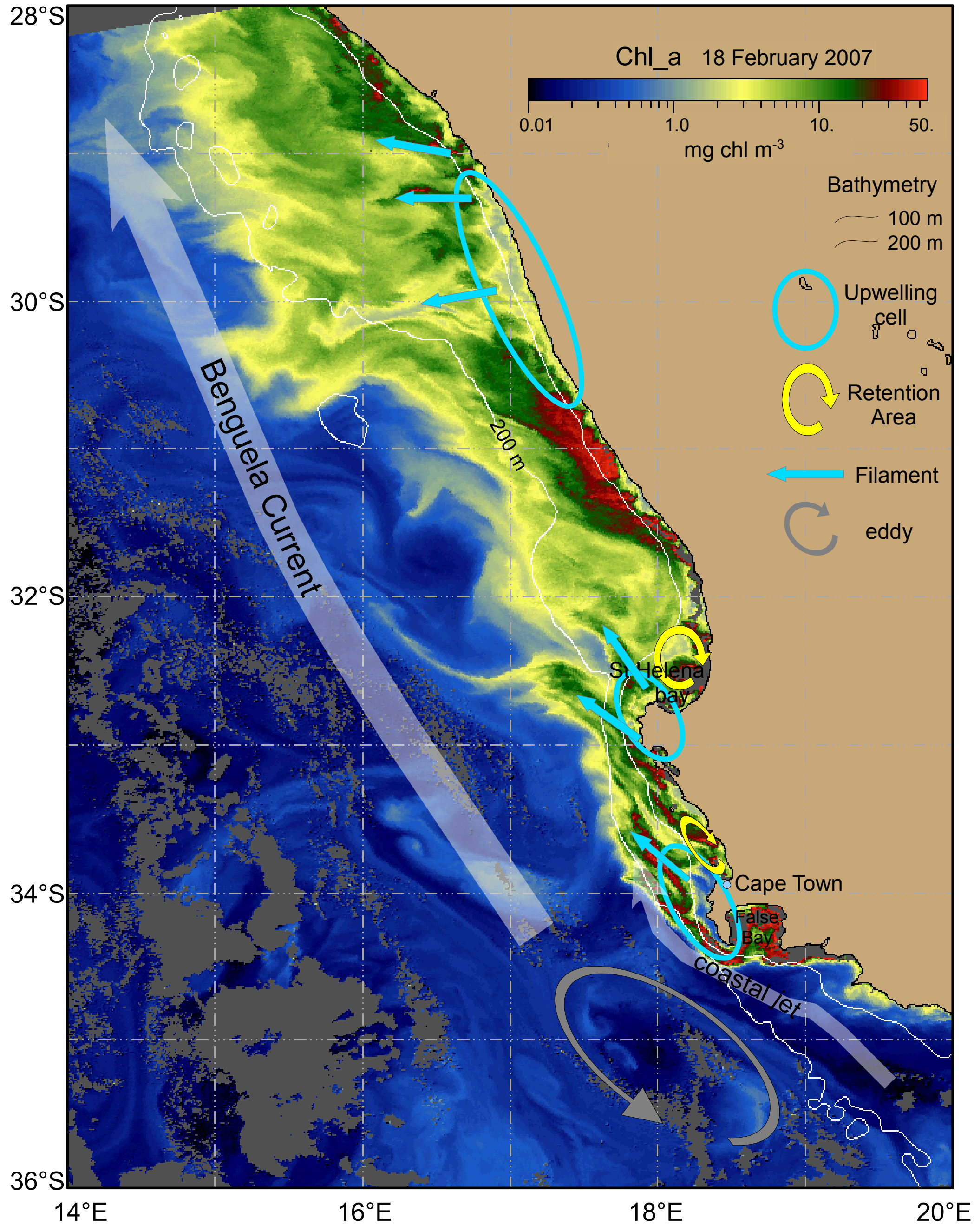

Figure 14.4 Same as Figure 14.2b (Chl-*a*) but using a colour palette. Note the logarithmic scale that accounts for the irregular distribution of the chlorophyll values. MODIS data provided by NASA/GSFC.

14.4 Answers

A1: The SST field (Figure 14.3) provides a synoptic view of the near surface dynamics, where upwelled waters are much colder than the surrounding waters. The minimal

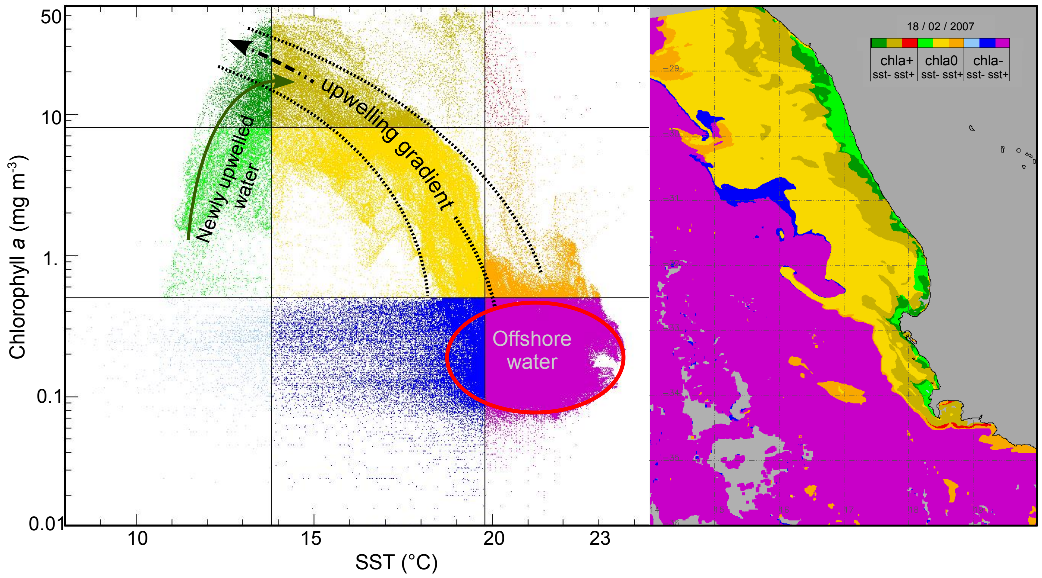

Figure 14.5 Cluster plot of the SST and SCC values showing a general negative relationship between the two parameters, as well as the intermediate chlorophyll and low temperature values of the newly-upwelled waters. MODIS data provided by NASA/GSFC.

temperature at the centre of the most active upwelling cell is close to 10°C, a temperature that is usually found at a depth of >100 m (data not shown), suggesting that the origin of the upwelled water is close to the continental slope. Several distinct upwelling cells occur at specific locations where the wind component parallel to the coast is maximum, according the Ekman pumping theory. The SST difference between the cool upwelled water and the warm offshore water is close to 10°C. This temperature difference can also be used as a proxy to estimate the intensity of the coastal upwelling, or at least its thermal impact at the sea surface, complementing the Ekman upwelling index, a measurement of the upwelling intensity computed from Ekman theory. A closer look at the concomitant weekly wind field (insert in Figure 14.2) shows that the location of the three identified upwelling cells matches exactly with those coastal portions parallel to the wind direction, where the upwelling process is maximal, according the Ekman theory (Figure 14.1a).

A2: The location, intensity and shape of the thermal fronts associated with these coastal waters supplies a lot of information on the mesoscale circulation features and the influence of the coastline. Knowledge of the bathymetry (100 and 200m isobaths) is essential to study the effects of the continental shelf and to understand the forcing effects of the large scale circulation (the westward coastal jet in the southern part of the area). A long upwelling filament (~200 km), situated between 32 and 33°S is clearly visible on the SST image, as well as the chlorophyll image (Figures 14.3 and 14.4). Many other filaments are visible, all associated with the various upwelling cells identified. Outside the coastal upwelling area, a warm anticyclonic eddy is clearly visible (grey arrow), partly generated by the frictional forces of the coastal jet current. Its central region, situated at 35°S and 18°E, is characterized by very low chlorophyll concentrations. This characteristic can be attributed to the deepening of the isotherms as a result of the surface convergent field associated with the "spinning up" of the eddy. An excellent description of eddies, as well as their importance as a temporary habitat for marine fish larvae, can be found in Bakun (2006).

A3: The surface chlorophyll field (Figure 14.4) provides an informative view of the biological response to surface enrichment resulting from coastal upwelling. At first glance, we observe a clear inverse relationship between SST and SCC, which is called the "upwelling gradient". Figure 14.5 summarize what we can deduce from a careful observation of both the SST and SCC fields from Figures 14.3 and 14.4. The colours in Figure 14.5 represent 9 partitions of the relationship between the two variables, as well their spatial correspondence. The warm "offshore waters" are easily identified by temperatures >20°C and low chlorophyll concentrations ($<$ 0.5 to 0.6 mg m^{-3}). When moving towards the coast, the main category of water is that associated with the "upwelling gradient", where we can observe the progressive transformation of the recently-upwelled water (shown in green) as it reaches the euphotic layer. The chlorophyll concentration in this water mass increases progressively as photosynthesis takes place and the phytoplankton cells increase in number. The maximum chlorophyll values are extremely high (close to signal saturation). Chlorophyll concentration generally decreases as the water drifts offshore because of the "dilution" of the upwelled water. This upwelling gradient is maximum in the coastal area for high chlorophyll values $>$ 10 mg m^{-3} (dark green and brown-green colours) before nutrients start to become a limiting factor for algae growth. To fulfill the view of this ecological gradient we may imagine the role of the zooplanktonic grazers (mainly large copepod species) that feed actively on the large diatom cells commonly found in upwelling areas. Similarly, small pelagic fish such as anchovies feed on the copepods. This chain of events evolves both in time and space, along a cross-shore gradient of progressively more mature waters.

A4: A closer look at the centre of the upwelling cells (particularly those off the Cape coast, indicated by blue rings) shows very low values of SCC as opposed to the previously observed negative relationship between SCC and SST. This surprising result can be explained by the residence time of the water masses in the euphotic layer, which is too short (less than a few days) to allow for a significant multiplication of the algae (diatoms in our case). Effectively, the time for cell division to take place is about 5 days. Further offshore, where the residence time at the surface becomes higher, photosynthesis takes place, the cells multiply and the chlorophyll concentration increases. A typical time period for a chlorophyll increase from 1 mg

m^{-3} to 10-20 mg m^{-3} in this area is 6-7 days (Brown and Hutchings, 1987).

A5: Any particle (e.g. phytoplankton cell, fish larvae) close to an upwelling cell has a high probability of being driven rapidly far offshore, especially if it is retained in an upwelling filament. In contrast, certain areas in this region make it possible for the same particles to be retained in a favourable environment for days or even weeks. The coastal complexity and the presence of capes induce such privileged areas. This is the case in St Helena Bay (indicated as a "retention area" in Figure 14.3) as well as the bay of Cape Town. Further south, False Bay provides a good retention area, combining relatively warm water associated with a strong enrichment, horizontally advected from coastal counter currents. This area is known for its high species diversity, including seals, white sharks, and even surfers!

14.5 References

14.5.1 Information for downloading data used in this case study

- MODIS data general access (ordering "Level 2" data): `http://oceancolor.gsfc.nasa.gov/cgi/browse.pl`
- Direct access to 1-km full orbit "Level 2" MODIS chlorophyll and SST data: `http://oceandata.sci.gsfc.nasa.gov/MODISA/L2/`
- SeaWinds data and "browse" images can be downloaded in various formats from `http://podaac.jpl.nasa.gov/DATA_CATALOG/quikscatinfo.html`
- "Level 3" gridded data in HDF4 format, along with various decoding software in C, Fortran, IDL and MATLAB: `http://aspera.jpl.nasa.gov/download/pub/ocean_wind/quikscat/L3/`

14.5.2 Information for related data and documentation

- Aqua sensor: `http://aqua.nasa.gov/`
- MODIS ocean colour products: `http://picasso.oce.orst.edu/ORSOO/MODIS/code/Table1Products.html` (see also `http://oceancolor.gsfc.nasa.gov/DOCS/MSL12/master_prodlist.html/` for more detailed information)
- EOS products: `http://eospso.gsfc.nasa.gov/eos_homepage/for_scientists/index.php`
- The Earth Science Reference Handbook: (291 pages, 7.5 MB, PDF document) `http://eospso.gsfc.nasa.gov/ftp_docs/2006ReferenceHandbook.pdf`
- SeaWinds products: `http://podaac.jpl.nasa.gov/DATA_CATALOG/quikscatinfo.html`
- Ready to use data series: some of the data included in this case study was extracted from the AOOS web site (`http://aoos.mpl.ird.fr/`), a satellite image series finder, developed at IRD, Institut of Research for Development by the CRH (Centre de Recherches Halieutiques).

14.5.3 References and Suggested Reading

Ekman WK (1905) On the influence of earth's rotation on ocean currents. Arkiv för Matematik, Astonomi och Fysik 2 (11): 1956

Bakun A (1975) Daily and weekly upwelling indices, West coast of North America, NOAA Technical Reports, NMFS SSRF-693, 1967-73

Bakun A (2006) Front and eddies as key structures in the habitat of marine fish larvae: opportunity, adaptative response and competitive advantage. Scientia Marina, 70S2: 105-122

Brown PC, Hutchings L (1987) The development and decline of phytoplankton blooms in the southern Benguela upwelling system. 1. Drogue movements, hydrography and bloom development. In: Payne AIL, Gulland JA, Brink KH (Eds), The Benguela and Comparable Ecosystems, S Afr J Mar Sci 5:357-391

Brown OB, Minnett PJ (1999) MODIS Infrared Sea Surface Temperature Algorithm Theoretical Basis Document, Ver 2.0 http://modis.gsfc.nasa.gov/data/atbd/atbd_mod25.pdf

Carder KL, Chen FR, Cannizzaro JP, Campbell JW, Mitchell BG (2004) Performance of the MODIS semi-analytical ocean color algorithm for chlorophyll-a. Adv Space Res 33:1152-9

Demarcq H, Faure V (2000) Coastal upwelling and associated retention indices from satellite SST. Application to Octopus vulgaris recruitment. Oceanol Acta 23(4):391-408

Demarcq H, Barlow R, Hutching L (2007) Application of a chlorophyll index derived from satellite data to investigate the variability of phytoplankton in the Benguela ecosystem. Afr J Mar Sci 29(2):271-282

Lasker R, Pelaez J, Laurs RM (1981) The use of satellite infrared imagery for describing ocean processes in relation to spawning of the northern Anchovy (*Engraulis mordax*). Rem Sens Environ 11:439-453

O'Reilly JE and 24 co-authors (2000) SeaWiFS Postlaunch Calibration and Validation Analyses, Part 3. NASA Tech Memo 206892, 11: NASA Goddard Space Flight Center, Greenbelt, Maryland

Tang W, Liu WT Stiles BW (2004) Evaluation of high-resolution ocean surface vector winds measured by QuikSCAT Scatterometer in coastal regions. IEEE 2(8):1762-1769

Van der Lingen C, Fréon P, Hutchings L, Roy C, Bailey G, Bartholomae C et al. (2006) Forecasting shelf processes of relevance to marine resources in the BCLME. In: Rizzoli P, Woods J (Eds). The Benguela: Predicting a Large Marine Ecosystem. Elsevier Series

Walton CC, Pichel WG Sapper JF (1998) The development and operational application of nonlinear algorithms for the measurement of sea surface temperatures with the NOAA polar-orbiting environmental satellites. J Geophys Rese 103(C12):27,999-28,012

Case Study 15

Comparison of *In Situ* and Remotely-Sensed Chl-*a* concentrations: A Statistical Examination of the Match-up Approach

E. Santamaría-del-Ángel*[1], R. Millán-Núñez[1], A. González-Silvera[1] and R. Cajal-Medrano[1]

15.1 Background

With the launch of the Coastal Zone Color Scanner (CZCS) in November of 1978, a new era in oceanographic studies began. This was the first instrument dedicated to the measurement of ocean colour using satellite imaging, and its main purpose was to determine whether spectroradiometric observations could be used to identify and quantify suspended or dissolved matter in ocean waters (IOCCG, 2000; 2004; 2006). CZCS imagery encompassed large geographic areas and was collected over short periods of time, something that was not possible with previous measurement techniques (ships, buoys, airplanes). CZCS was a 'proof-of-concept' mission, to determine whether Chlorophyll-*a* concentration (Chl-*a*) could be estimated from space, based on spectrophotometric principles. Studies using CZCS data (Peláez and McGowan 1986; Yoder et al., 1987; Muller-Karger et al., 1991; Santamaría-del-Ángel et al.1994a,b) showed that measurement of the colour of the ocean is a powerful tool for oceanographic studies, and that this method can yield information about the ocean surface at meso- to macro-scales. These studies provided justification to launch other sensors such as SeaWiFS (Sea-viewing Wide Field-of-view Sensor), MODIS-Aqua (MODerate resolution Imaging Spectroradiometer) and MERIS (MEdium Resolution Imaging Spectrometer).

Data extracted from ocean-colour images allows one to examine the temporal-spatial variability of the surface layer of the oceans. For example, Chl-*a* is an index of phytoplankton biomass, so a time series of Chl-*a* concentrations can be used in modelling studies that require phytoplankton biomass as an entry variable, such as primary productivity models (Platt et al. 1988; Barocio-León et al., 2007) or carbon

[1]Facultad de Ciencias Marinas, Universidad Autónoma de Baja California (FCM-UABC) Carretera Tijuana-Ensenada Km 106 C.P. 22860 Ensenada BC. Mexico. * *Email address:* santamaria@uabc.edu.mx

flux models (Camacho-Ibar et al., 2007). In addition, ocean-colour images can provide information about oceanographic surface structures at the meso-scale and allow for tracking of their space-time variations (Traganza et al. 1980; Santamaría-del-Ángel et al., 2002; González-Silvera et al., 2004, 2006; López-Calderón et al., 2008). Such technology may also be able to provide data for fishery studies (IOCCG, 2009; Dulvi et al., 2009).

One of the main challenges in using ocean-colour imagery is to determine the degree of correlation between the *in situ* measurements and the satellite-derived data. NASA uses the 'match-up' technique, which is based on a hypothetical linear relationship between satellite Chl-*a* concentrations ($Chla_s$) and the *in situ* values obtained from water samples ($Chla_i$). For most data, a 70% correlation (or 30% error) is considered a good fit (Gregg and Casey, 2004; Djavidnia et al., 2006). To understand the match-up approximation, and to consider the pros and the cons of this method, several statistical considerations must be taken into account: (a) the pattern of data variability, (b) the association indexes used to express the relationship between the *in situ* and satellite data, and (c) the number of data points considered when applying this approximation. It is also important to consider the data scales e.g., *in situ* measurements are generally based on ~1 liter of sea water, while remotely-sensed estimations are obtained from an area of ~1 km^2. It is difficult to obtain an ideal match-up in space and time. Ideally, *in situ* measurements should be collected at the same time as the radiometric measurements required to validate ocean-colour algorithms.

The spatial distribution of phytoplankton on the ocean surface is not homogeneous; similarly, the vertical distribution in the water column is not homogeneous and generally exhibits a sub-surface maximum (Cullen and Eppley, 1981; Millán-Nuñez et al., 1996). The distribution and size of the patches depends on a number of physical (light, turbulent mixing processes such as wind, surges), chemical (nutrients) and biological (algal type) factors. The $Chla_s$ data provides information about the phytoplankton biomass in the first optical depth at a scale of ~1 km per pixel (Figure 15.1) while the $Chla_i$ data are derived from discrete bottle samples near the ocean surface. Differences in sampling techniques are one of the factors contributing to the variability of the two datasets. Both approximations seek the concentration of Chl-*a*, but while the *in situ* samples are based on spectrophotometric, fluorometric, or HPLC determinations of ~1 liter of water, remote sensor measurements integrate data (through marine optics approximations) from a greater volume, yielding average values of Chl-*a* concentration (Fig. 15.1). Thus the *in situ* and remote sensor measurements evaluate processes on different space/time scales (Fig. 15.2). Satellite remote sensing allows the study of processes >10 km horizontal scale, encompassing several decades, while *in situ* measurements study processes over a much smaller time and space scales (cm to meters, minutes to days).

The 'match-up approximation', a graphical technique based on a theoretical straight line fitted to two variables with identical distribution patterns, can be used

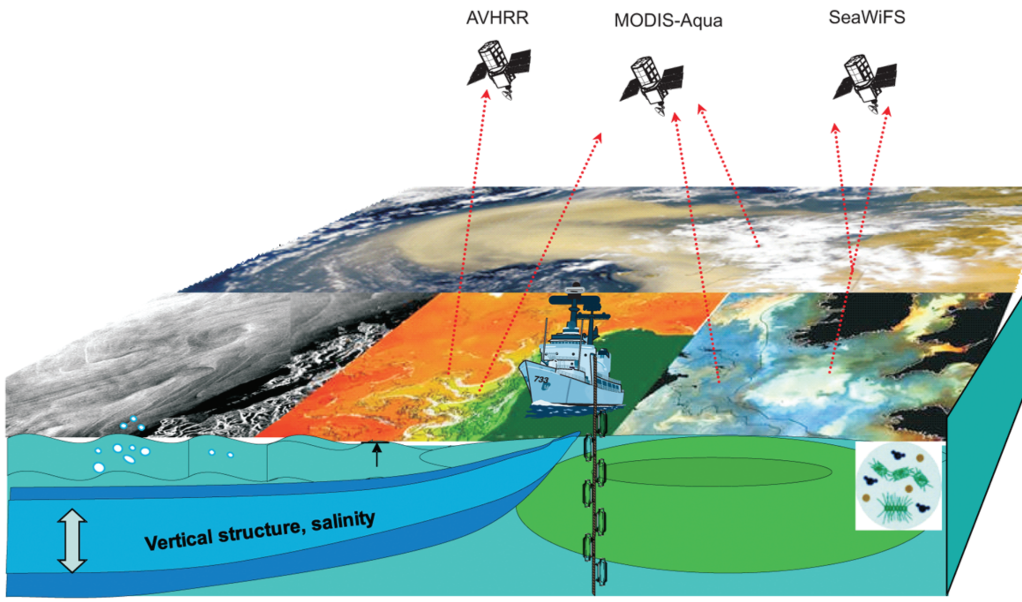

Figure 15.1 Schematic representation of the *in situ* and satellite-based sampling methods.

to compare data. If one variable is plotted against itself, or two variables with different magnitudes are plotted, the resulting graph yields a straight line with a 45-degree slope. As the data distribution differs, the dispersion increases. To determine the statistical validity of the observed patterns, a statistical analysis can be applied to examine the level of linear association between variables. The most common linear association index is Pearson's correlation coefficient (r_P), often simply just called 'correlation coefficient', denoted r. The mathematical expression is:

$$r_P = \frac{\mathrm{Cov}_{A,B}}{SD_A \times SD_B} \tag{15.1}$$

where r_P = Pearson's correlation coefficient; $\mathrm{Cov}_{A,B}$ = Covariance of A and B; SD_A = standard deviation of A; SD_B = standard deviation of B. It is a measure of the correlation (linear dependence) between two variables A and B, giving a value between +1 and -1 inclusive (1 indicates a direct linear relationship, -1 indicates an inverse linear correlation, and zero indicates no linear relationship). It is expressed by the covariance of the two variables divided by the product of their standard deviations. A hypothesis test known as a 'correlation analysis' is carried out to determine if the coefficient is significant:

$$H_0 : r_P = 0$$
$$H_a : r_P \neq 0$$

To accept or reject H_0, two values must be compared; the calculated value ($r_{P_{cal}}$),

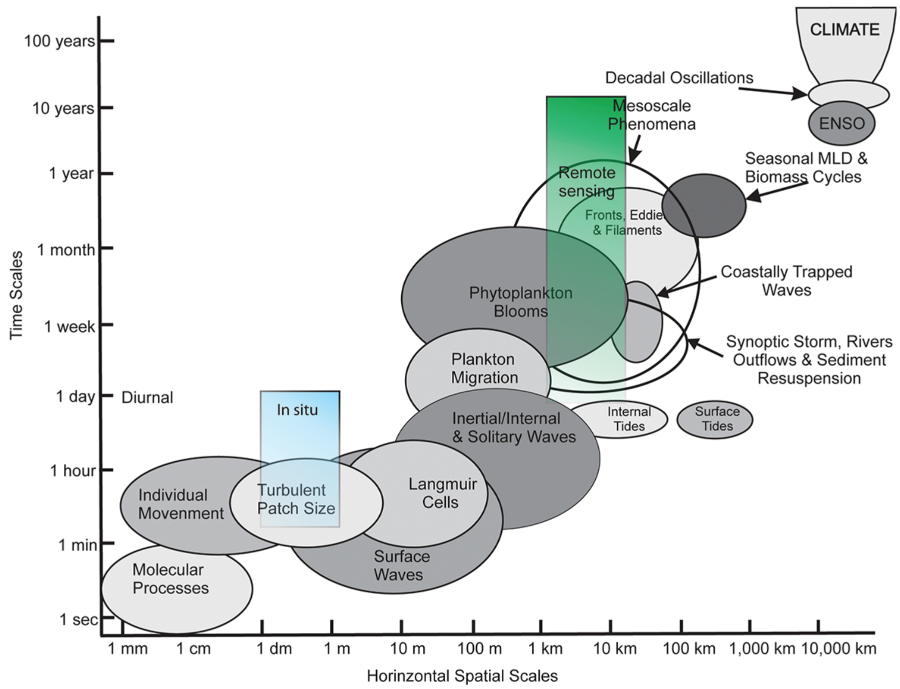

Figure 15.2 Schematic representation of the temporal space scales that cover each type of sampling method.

derived from Equation 15.1, and the critical value ($r_{P_{cr}}$) obtained from a table of critical values (found in any statistical textbook) based on the degree of freedom (df = n-1) and the error α (1-confidence level). Confidence levels are 90, 95 and 99% yielding errors of 10, 5 and 1, respectively. $r_{P_{cr}}$ is the minimum significant value of r_P. If $r_{P_{cal}} > r_{P_{cr}}$, H_0 is rejected and is statistically significant. If $r_{P_{cal}} < r_{P_{cr}}$, H_0 cannot be rejected and r_P is not significant. Decision making becomes more robust with a greater number of data points, which is why the number of data points is critical. In general, only a small number of data points are obtained if one uses only the samples collected close the time of the satellite overpass, or on sunny days.

A significant value does not imply a cause-and-effect relationship. For example, a correlation coefficient of 0.975 between Chl-*a* and sea surface temperature (SST) does not imply an increase of Chl-*a* with an increase in temperature, but rather that SST can be used an indicator of temperature surge e.g. upwelled cool nutrient-rich water can cause an increase in the phytoplankton biomass in the euphotic zone. Furthermore, it should be noted that $Chla_s$ is expressed on a logarithmic scale while r_P is not, so a logarithmic transformation of the Chl-*a* data is required. To perform the match-up in a more direct manner, the use of Spearman's Non-Parametric Correlation Coefficient can be used (Equation 15.2):

$$r_S = \frac{\mathrm{Cov}_{\mathrm{RA,RB}}}{SD_{\mathrm{RA}} \times SD_{\mathrm{RB}}} \tag{15.2}$$

where: r_S = Spearman's correlation coefficient; $\mathrm{Cov}_{\mathrm{RA,RB}}$ = covariance of the ranges of A and B; $\mathrm{SD}_{\mathrm{RA}}$ and $\mathrm{SD}_{\mathrm{RB}}$ = standard deviation of the ranges of A and B, respectively. The outcome for r_S is very similar to that of r_P, with a range of -1 to 1. The statistical significance of r_P can be determined through hypothesis testing similar to the tests described for r_S using a table of critical values of Spearman's coefficient. Case studies of two cruises are presented below as a practical demonstration:

1. **Case Study 1:** Only oceanographic stations sampled close to the time of the sensor overpass are considered, using data from the R/V IOFFE 2002 Ushuaia-Montevideo cruise (8-12 March, 2002).
2. **Case Study 2:** A combination of ten cruises in the CalCOFI (California Cooperative Oceanic Fisheries Investigations (`http://www.calcofi.org`) region is used from 2004 to 2006, sampled during daylight hours using both MODIS-Aqua and SeaWiFS data to help increase the number of observations.

SeaWiFS images with 1-km pixel resolution were used to make daily composites for both cruises. The concentration of Chl-*a* was calculated using the OC4-V4 algorithm (O'Reilly et al. 2000, Equations 15.3):

$$\mathrm{Chla} = 10^{0.366-3.067R+1.930R^2+0.649R^3-1.532R^4}, \tag{15.3}$$

where $R = \log_{10}\left[\frac{R_{\mathrm{rs}}443 > R_{\mathrm{rs}}490 > R_{\mathrm{rs}}510}{R_{\mathrm{rs}}555}\right]$. The OC3M-V4 algorithm was used for the MODIS-Aqua images (O'Reilly et al. 2000, Equation 15.4):

$$\mathrm{Chla} = 10^{0.283-2.753R+1.457R^2+0.659R^3-1.403R^4}, \tag{15.4}$$

where $R = \log_{10}\left[\frac{R_{\mathrm{rs}}443 > R_{\mathrm{rs}}488}{R_{\mathrm{rs}}551}\right]$.

15.2 Demonstration

15.2.1 Case Study 1

In situ data for this case study was collected during the R/V IOFFE Ushuaia-Montevideo cruise (8–12 March 2002) (Fig. 15.3), and was compared to SeaWiFS satellite data. Of the 337 oceanographic stations sampled during the cruise, only 14 fulfilled the requirements for match-up analysis i.e. samples collected between the hours of 10:00 and 14:00 (i.e. 2 hours before or after SeaWiFS overpass). In cases where the study area has high cloud coverage, all available satellite images are needed for analysis. Furthermore, some satellite images may not be centered directly over the sampling area, so some *in situ* sampling stations may not have adequate satellite data because of pixel degradation at the extreme edge of the sensor sweep (see Figure 15.4). In addition, clouds can prevent satellite data collection over a sampling station. It is thus recommended that a 3×3 pixel box centered over the station coordinates be used when extracting satellite data over a sampling station. There are several data extraction software packages available, including MatLab, WIM, ENVI and SEADAS.

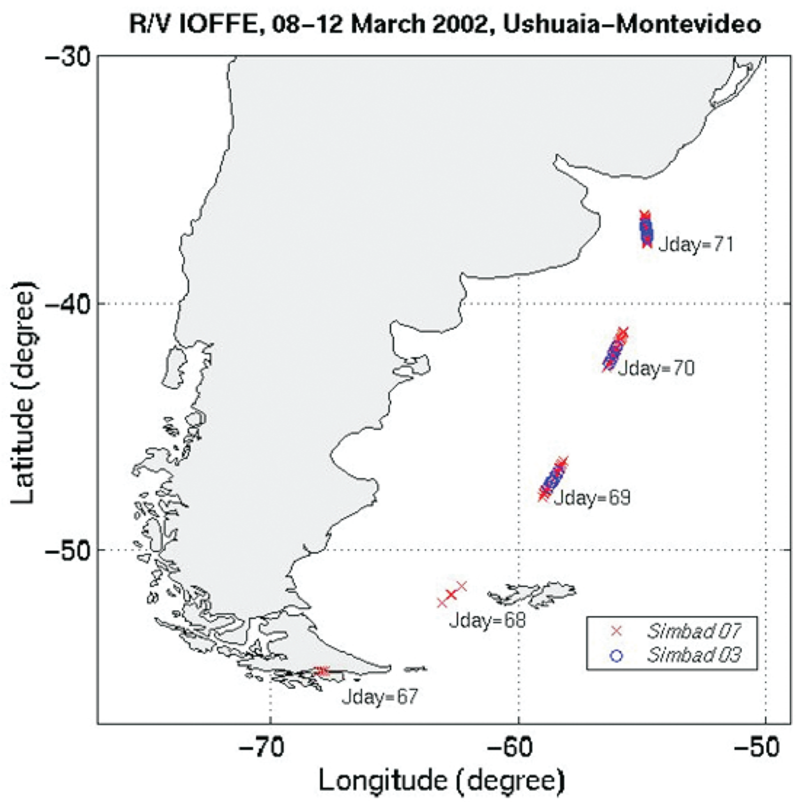

Figure 15.3 Study area of the R/V IOFFE Ushuaia-Montevideo cruise (8–12 March 2002).

All files used in this case study can be downloaded from the IOCCG website at http://www.ioccg.org/handbook/matchup/. The Excel file 'case1data.xls' shows 14 stations with $Chla_i$ (determined by HPLC) and the averages of the 3×3 box centered over the sampling station coordinates ($Chla_s$). Since $Chla_s$ represents integration over the first optical depth, samples within the first optical depth must be integrated for $Chla_i$. The correlation between $Chla_s$ and $Chla_i$ is determined using r_P. Although 14 data points is a relatively small number, $r_P = 0.852$ indicating that 85.2% of the total variability can be explained by one, or several, linear models. This value is statistically significant ($\alpha = 5\%$, $r_{P_{cr}} = 0.532$). Figure 15.5a shows that both *in situ* and satellite chlorophyll concentrations around 0.3 mg m^{-3} are remarkably similar. However, when $Chla_i > 0.6$ mg m^{-3} , $Chla_s$ is underestimated.

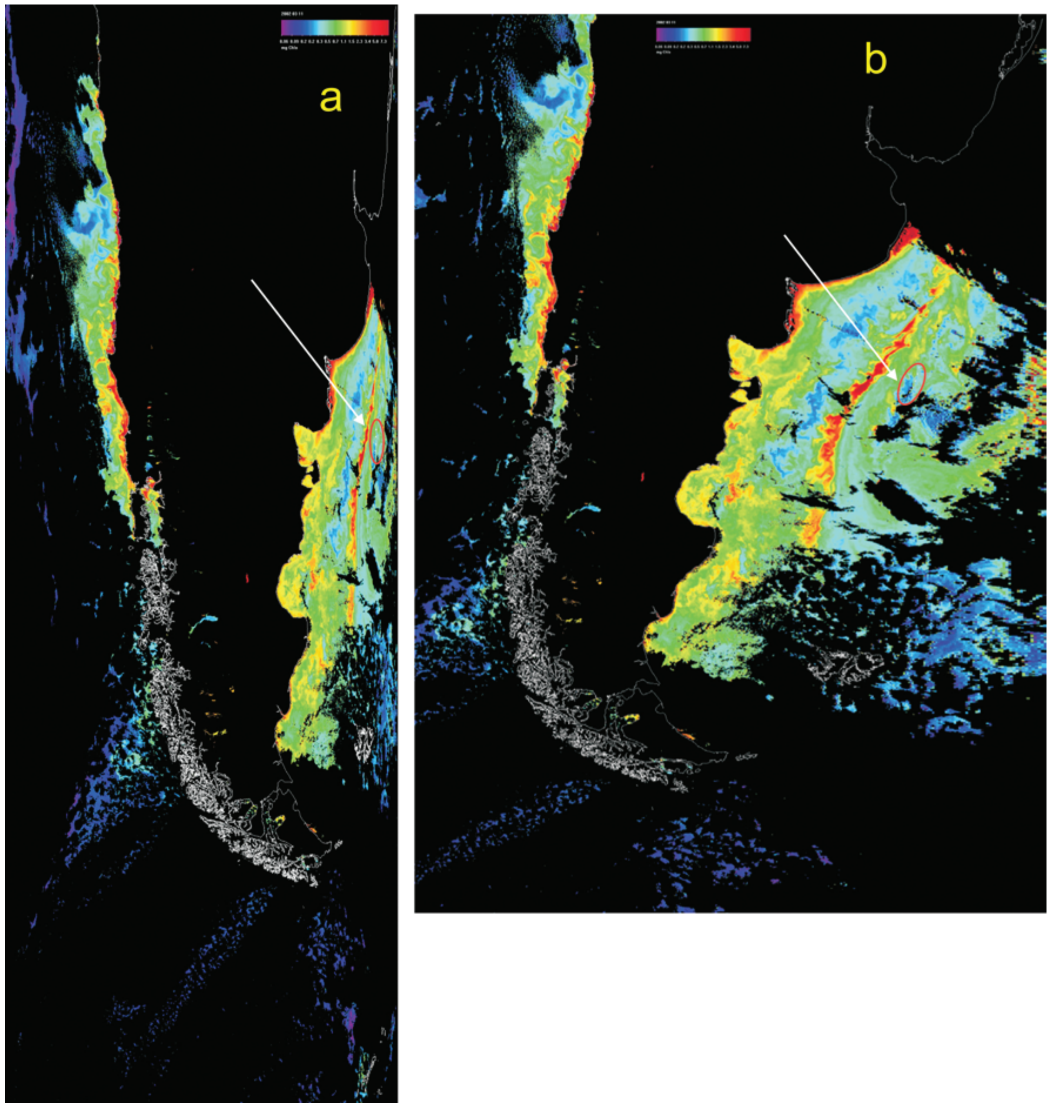

Figure 15.4 Example of SeaWiFS chlorophyll image S2002070154515 processed to (a) Level 2, and (b) Level 3.

15.2.2 Case Study 2

This example will demonstrate how to increase the number of matchup data points in areas with high cloud coverage, using data from more than one satellite sensor. Data from 10 cruises in the CalCOFI region were used (2004 to 2006) in conjunction with MODIS-Aqua and SeaWiFS satellite imagery (Figure 15.6). Using data from two satellite sensors increases the possibility of matchup data over a given sampling station because of the different overpass times of the sensors, and changes in cloud cover patterns throughout the day. Figure 15.7 shows SeaWiFS and MODIS-Aqua images for 7 and 8 February 2006. A common area is defined by a yellow circle in

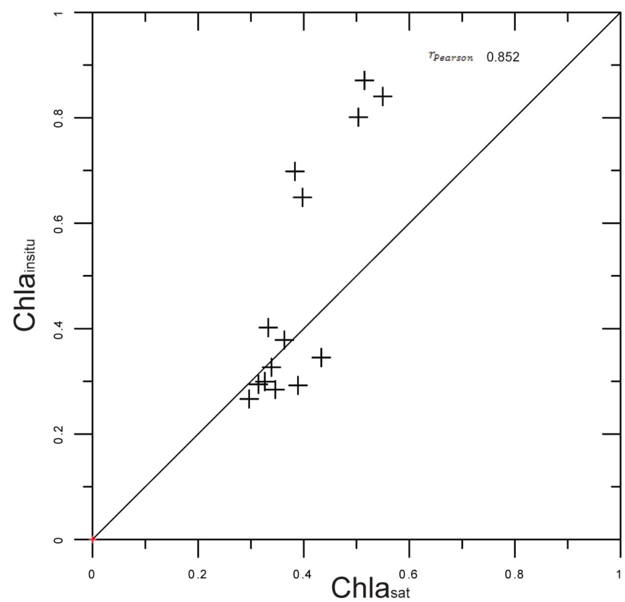

Figure 15.5 Relationship between *in situ* chlorophyll measurements from the R/V IOFFE cruise, and satellite SeaWiFS-derived chlorophyll.

each image to highlight changes in cloud cover patterns. The database for this case study can be found in the Excel file 'case2data.xls' on the IOCCG website. There are five columns: station-cruise, Chla$_s$ for MODIS-Aqua and SeaWiFS, the geometric mean of both, and Chla$_i$. The arithmetic mean ($\bar{X}_a$) for each station is the sum of the data values divided by the total number of data points.

$$\bar{X}_a = \frac{\Sigma x}{n} \tag{15.5}$$

This mean uses all pixels, even those with no geophysical values, so the geometric mean ($\bar{X}_g$) should be used to generate a value that is representative of the data:

$$\bar{X}_g = \frac{\Sigma x}{N_{\text{in}}} \tag{15.6}$$

i.e., the ratio of the sum of the valid data and the number of pixels that yielded these valid data points (N_{in}). Using equations 15.1 and 15.2, r_P and r_S coefficients were calculated for the data as well as the base 10 log-transformed data (Table 15.1). Using only the MODIS-Aqua satellite data for the 10 cruises over almost 3 years would yield 128 match-up data points. If only SeaWiFS data were used, this number would increase to 142. Combining data from the two sensors and using the geometric mean, the number of data points increases to 172. Note that all the coefficients are statistically significant at α = 5%; but only at concentrations < 1 mg Chla m^{-3}.

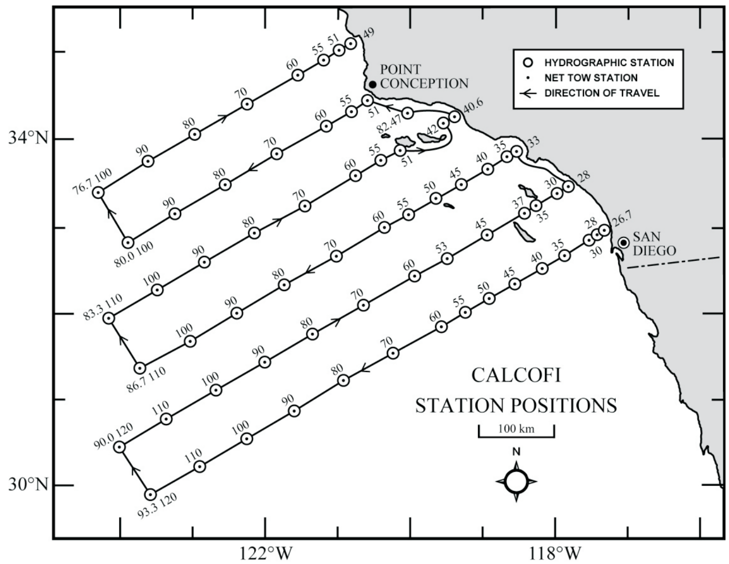

Figure 15.6 Location of the CALCOFI study area.

Table 15.1 Correlation between the *in situ* concentrations of chlorophyll-*a* and the concentrations derived from MODIS-Aqua, SeaWiFS and the combination of both sensors for CalCOFI cruises from 2004 to 2006.

	Data		Log_{10} Data	
	r_P	r_S	r_P	r_S
MODIS-Aqua (n=128)	0.690	0.839	0.807	0.839
SeaWiFS (n=142)	0.588	0.859	0.802	0.859
Both (n=172)	0.664	0.882	0.834	0.882

Since r_P determines the degree of correlation expressed by the variability explained by linear relationship, while r_S determines the degree of correlation (including that explained by linear models), Spearman values will be greater than Pearson values, which is apparent in the non-transformed data. $Chla_s$ is generally expressed on a logarithmic scale and it can be seen that r_P increases if the data is log-transformed, while r_S remains the same, suggesting that Spearman's correlation coefficient is better for establishing the degree of correlation between $Chla_i$ and $Chla_s$. Figure 15.8a shows that with non log-transformed data at low chlorophyll concentrations, there appears to be a high correlation between the satellite and $Chla_i$ data, but at concentrations > 1 mg Chl a m^{-3}, data dispersion increases considerably. This is less evident when expressing the same relationships on a logarithmic scale (Figure 15.8b). Note that expressing these relationships on a log scale only changes the visual representation, not the distribution pattern of the data points. Sampling can only provide a window of data into the global variability (Figure 15.8b gray

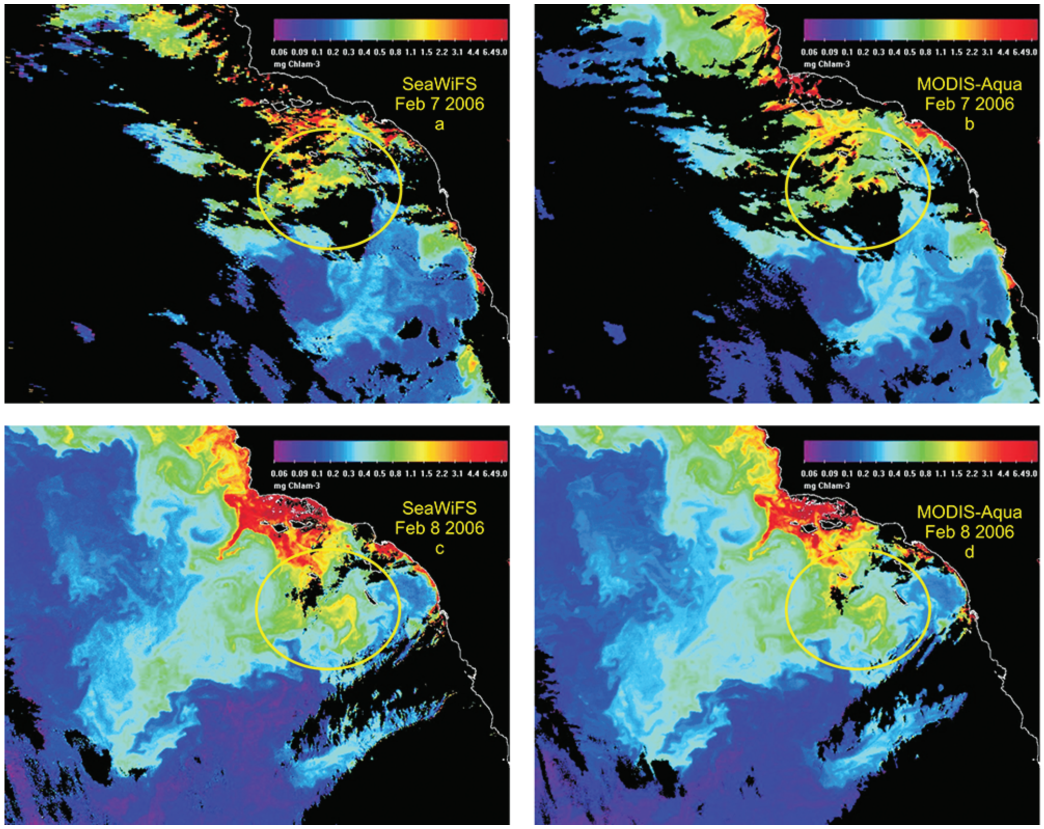

Figure 15.7 Example images for the CalCOFI case study from 7–8 February 2006. a) SeaWiFS image from 7 February 2006, b) MODIS-Aqua image from 7 February 2006, c) SeaWiFS image from 8 February 2006, and d) MODIS-Aqua image from 8 February 2006. The yellow circle delineates an area to examine variability in cloud coverage.

squares), which is why linear relationships cannot explain all cases. For this reason, Spearman's correlation coefficient is a better indicator than Pearson's because it explores all types of relationships between two variables.

The CalCOFI region represents a system with a high space-time variability that is affected by climate fluctuations (Bograd et al., 2003). The increase in the water temperature and thermocline depth and the stratification of the water column are accompanied by changes in the populations of algae, invertebrates, zooplankton, fish and birds (Bograd et al., 2003). The CalCOFI database and the information derived from satellite imagery offers the potential to construct robust models that can explain the high variability of this area. This region is characterized by a strong oceanographic structure at the mesoscale, with the generation and evolution of meanders, eddies and filaments along the coast. The combination of data from several sources (including satellites and *in situ* measurements) in numerical models can be used to complement the descriptions of this variability at the mesoscale. Di

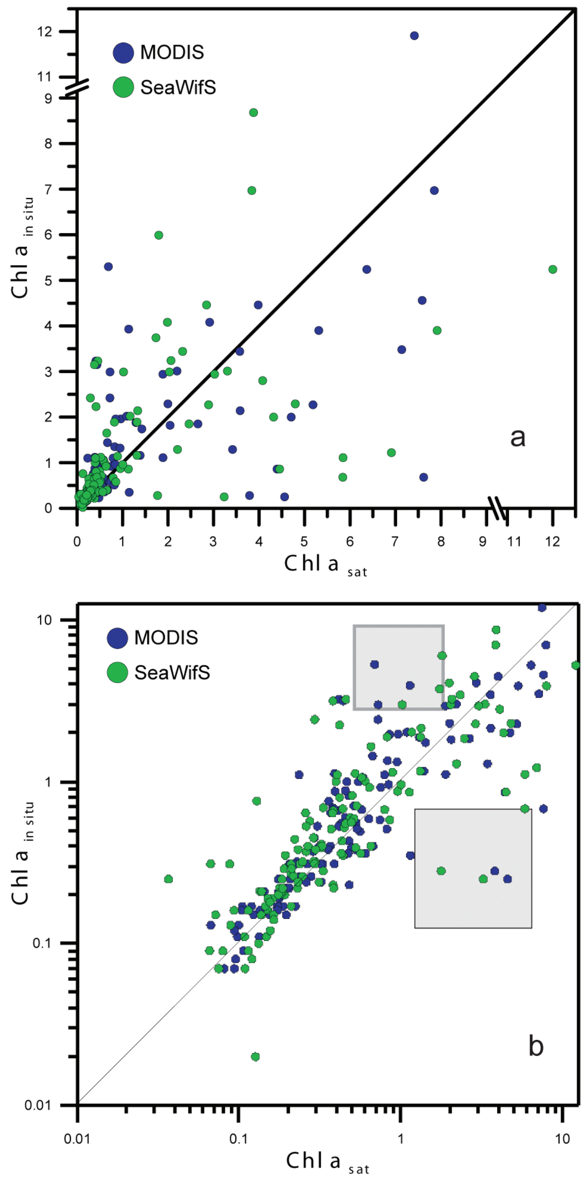

Figure 15.8 Relationship between *in situ* chlorophyll data and SeaWiFS (green circles) and MODIS-Aqua (blue circles) chlorophyll data for the CALCOFI cruises from 2004 to 2006, plotted on a linear scale (a), and a logarithmic scale (b). The grey squares represent a hypothetical window when using data from one cruise only.

Lorenzo et al. (2004) used the CalCOFI database in combination with data derived from SeaWiFS to model the dynamic nature of the California Current system. They noted that the comparison of *in situ* Chl-*a* data with that derived from SeaWiFS was difficult due to the different sampling scales employed by each approximation. This case study proposes a better approximation to compare the *in situ* and satellite data, allowing for the space-time resolution of both to be maximized.

15.3 Training

The files in the folder entitled "trainingfiles" (`http://www.ioccg.org/handbook/matchup/`) will be used in this section. First we will focus on data extraction from stations in the 3×3 pixel boxes. The stations and images of the CalCOFI 0507 cruise (July 2005) will be used. Before starting, three points must be considered:

1. It is important for all images to have the same geographic projection to facilitate preparation of the script for data extraction (based on latitude, longitude and geophysical value data matrices). If the images do not have the same projection, the matrices will have different dimensions.
2. The text file ’0507stations.txt’ lists the details of the sampling stations in three columns: longitude, latitude (both in degrees and tenths of a degree) and station identification. The first row is used for column headers. Note that latitudes are positive in the northern hemisphere and negative in the southern hemisphere, and longitudes are positive in the eastern hemisphere and negative in the western hemisphere.
3. A text file must be generated with a list of addresses where the images are stored (see ‘0507imagery.txt’).

We used the WIM (Windows Image Manager) software (`http://www.wimsoft.com`), specifically its WAM (WIM Automation Module) module called ‘wam_statist’. In the upper left hand corner, there is a window labeled "List of Images", where the file name ‘0507imagery.txt’ is placed. In the upper right hand corner, there are two windows: the top one is labeled "Mask or Station File Name" where the name and address of the station file (‘0507stations.txt’) is placed. The name and address of the file where the data are stored (‘0507wam_statist_result.csv’) is placed in the bottom window. This type of file can be opened in Excel and yields 23 columns. Column A consists of the image names, columns B and C are the start and end years (if the images are composites). Columns D and E are the start and end days (if the images are weekly or monthly composites). This case study uses daily LAC images with B and C values of 2005 and D and E having the same value (until another image is analyzed). Column F identifies the station that is named in the third column of the station file (‘0507stations.txt’). Column G indicates the number of pixels in the 3×3 box that have data (G, N_{in}) and column H indicates the number of pixels that do not have data (H, N_{out}). The maximum value in each column is 9 and the minimum is 0, so that if column G has a value of 9, all the pixels in the 3×3 box have data.

The basic geometric statistical parameters can be extracted from the data in column G, (based only on the valid pixels): minimum (I), maximum (J), mean (K), standard deviation (L), and median (M). When there are no data in the 3×3 box due to cloud coverage, signal saturation, or other factors (i.e. column H has a value of 9), the value in these columns is -99. Column N denotes the pixel centered in the geographical coordinates where the station was located. Columns P through W contain the values of the remaining pixels in the 3×3 box. These data allow comparisons to be made with other statistical parameters, e.g. the mode.

The next step is to generate a file where the extracted data can be combined with the *in situ* data. In this case, this file was generated by combining the data from CalCOFI cruise 0507 and the results of the extraction file '0507wam_statist_result.csv'. The resulting file ('0507match-up.xls') will be used in the second part of this section, where the focus will be on the calculation of Pearson's and Spearman's correlation coefficients to establish the degree of correlation between Chl_s and Chl_i. We will use data from MODIS-Aqua and SeaWFiS to increase the number of data points for the calculation of the two coefficients (using Equations 15.1 and 15.2), for both the log-transformed and raw data (Table 15.2).

Table 15.2 Correlation between *in situ* chlorophyll-*a* and chlorophyll derived from MODIS-Aqua, SeaWiFs, and the combination of the two sensors, for the CalCOFI 0507 cruise.

	Data		Log_{10}Data	
	r_P	r_S	r_P	r_S
MODIS-Aqua (n=5)	0.822	1.000	0.947	1.000
SeaWiFS (n=4)	0.933	1.000	0.881	1.000
Both (n=4)	0.873	0.964	0.946	0.964

Next, the statistical range must be calculated. This is done by labeling the smallest number in the data series 1, the next smallest 2 and so on, until the whole data series has been labelled. Table 15.3 shows three sets of data. Set A has no repeating values, so the range is calculated starting at 1 and ending in 10, since n = 10. Set B has repeating values (number 90 is repeated twice). The corresponding ranges would be 1 and 2, so a mean of the ranges is calculated and each would be assigned a value of 1.5 ($\frac{1+2}{2}$). The next range to assign would be 3. Set C has a triple repeat of 124 and a double repeat of 128. In this case, 124 would have the corresponding ranges 4, 5, and 6, so a mean range of 5 is assigned to each, leaving the next range value as 7. For the 128 repeat, the corresponding ranges are 7 and 8 so a range value of 7.5 is assigned to each, leaving the next range value as 9.

Even with only a few data points (Table 15.2) Chl_s displays a high correlation with Chl_i. As noted previously, r_P coefficients are generally lower than r_S (= 100 in this study). Even when the r_P values are large, this does not imply a 1:1 relationship (Figure 15.9a). Rather, it implies that a high percentage of the variability can be explained by linear models. If the same graph is expressed on a log scale (Figure 15.9b), an apparent 1:1 linear relationship is observed. Note, the relationship of $Chla_s$ to $Chla_i$ is not the same as $\log_{10}Chla_s$ to $\log_{10}Chla_i$.

Table 15.3 Data demonstrating the calculation of ranges for one variable.

Set A	Rank A	Set B	Rank B	Set C	Rank C
133	6	129	6.0	128	7.5
137	8	132	8.0	124	5.0
99	3	90	1.5	110	3.0
138	9	136	9.0	131	9.0
92	2	90	1.5	98	2.0
89	1	93	3.0	84	1.0
130	4	114	4.0	147	10.0
132	5	129	6.0	124	5.0
141	10	150	10.0	128	7.5
135	7	129	6.0	124	5.0

If extrapolation of data (modelling one concentration based on the other) is desired in addition to generation of the linear model, tests on the significance of the intercept, the slope and the global significance of the model must be carried out. However, none of this is needed if only the degree of match-up is desired. r_P yields the degree of variability that can be explained by linear models. If one concentration is to be modeled based upon the other, the analysis can be based on empirical (linear) or mechanistic models. All the models have a determination coefficient (R^2); i.e. the percentage of variability explained by a specific model. It is calculated as follows:

$$R^2 = \frac{SSM}{SST_o} \tag{15.7}$$

$$SSM = \sum_{i=1}^{n} (\hat{y}_i - \bar{y})^2 \tag{15.8}$$

$$SST_o = \sum_{i=1}^{n} (y_i - \bar{y})^2 \tag{15.9}$$

where SSM is the sum of the squared differences between the modelled data ($\hat{y}_i$) and the mean of the observed data ($\bar{y}$). SST_o is the sum of the squares between the observed data (y_i) and the mean of the observed data ($\bar{y}$) and defines of the total variability of the dependent variable. R^2 is the ratio of the two sums of squares. When a linear model is used, it is assumed that $R^2 = r_P^2$, but this may not hold true for all data.

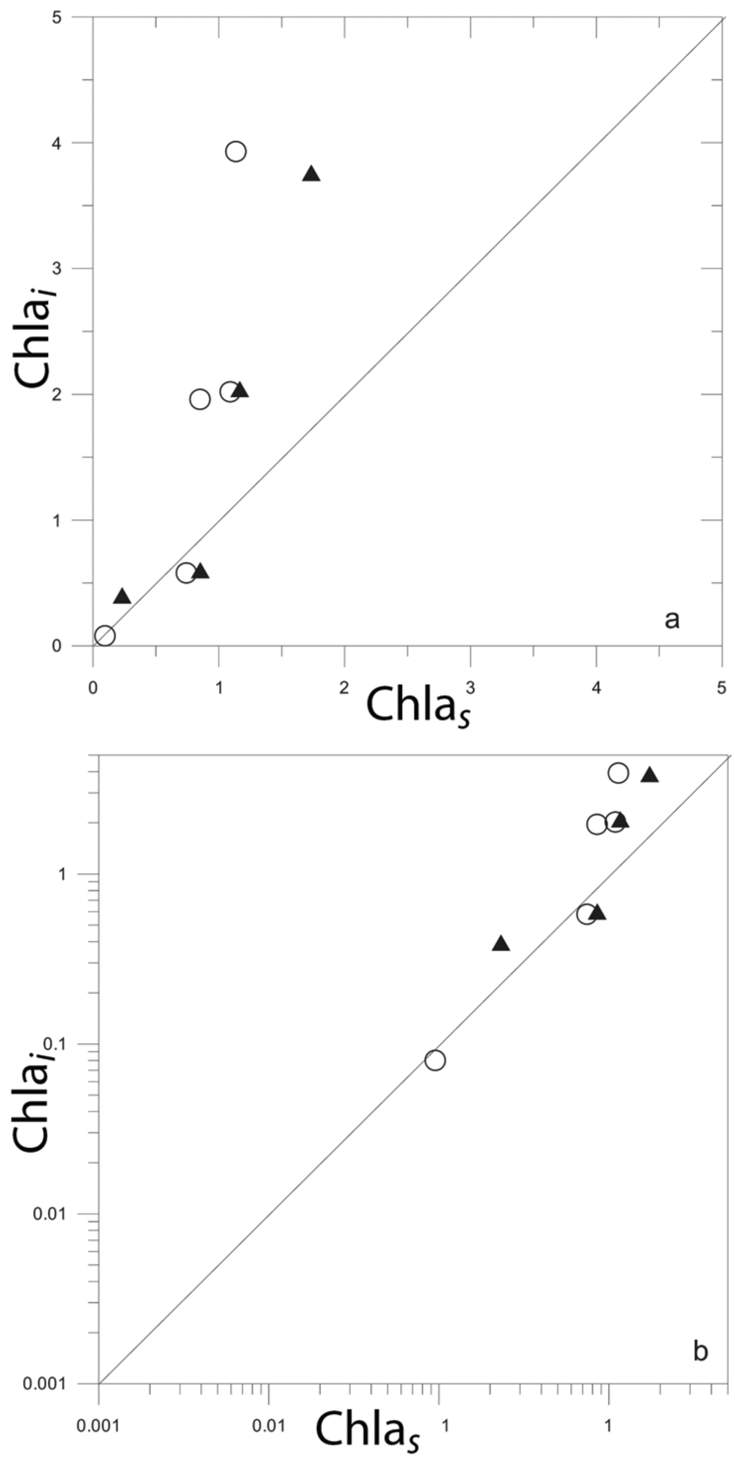

Figure 15.9 Correlation between *in situ* chlorophyll and satellite-derived chlorophyll (triangles = SeaWiFS; circles = MODIS-Aqua) for the CALCOFI 0507 cruise, plotted on a linear (a) and (b) logarithmic scale.

15.4 Questions

1. Why is it important to have an *in situ* database for a defined grid, sampled over a long period of time?
2. Why is the CalCOFI area so important in this regard?
3. What is the weakness of the CalCOFI database, and how can that weakness be minimized?
4. What are the advantages and disadvantages of using satellite-derived data in this area?
5. Why is the relationship between *in situ* measurements and those derived from remote sensors important?
6. Are "normalized" data required to carry out match-up approximations? Do they have to be normalized with logarithms?
7. How should match-up study results be expressed?
8. What is the difference between R^2 and r_P?
9. Is Spearman's coefficient better than Pearson's?
10. How do you calculate the range for r_S?
11. What is the geometric mean?
12. Is the geometric mean representative of the 3×3 data extraction box?
13. Why is it important to have all the images at the same projection?

15.5 Answers

1. This sampling scheme allows variations over seasons, years, decades and longer time scales to be assessed in a more reliable manner and also allows the system to be modelled.
2. The CalCOFI area has a sampling record, for a defined grid, going back more than 60 years A possible weakness of the CalCOFI database is that it only provides data four times a year, leaving nearly nine months with no monitoring in the area. The *in situ* observations of CalCOFI can be complemented with the use of ocean colour and SST images. Although these images only provide information about the surface of the ocean, they can provide a synopsis of changes in space and time.

3. Advantages include access to data on a daily time scale over a broad area, which allow the synoptic description of space-time variability and highlight oceanographic structures at the mesoscale. Currently, a long time series with a 1-km pixel size can be generated. Disadvantages of these data are that they only yield surface information and require cloudless days. Weekly or monthly data composites and long time series can be derived from remotely-sensed data.

4. The relationship between *in situ* measurements and those derived from remote sensors has three components: a) synoptic complementary data for space-time studies in windows where the *in situ* sampling does not yield any data; b) representation of indirect approximations, as well as those from remote sensors; and c) entry variables used to model the system.

5. No, if "normalized" means that the data fit a Gaussian distribution. Pearson's and Spearman's correlation coefficients do not require that the internal distribution of the variables fits a Gaussian curve.

6. The calculated value of the chosen coefficient must be presented as well as the significance given by the hypothesis tests, indicating the number of data points and the error, α. A graph can be constructed with axes that have the same scale. A 45° straight line denoting the 1: 1 line should be included.

7. r_P is the degree of variability that can be explained by linear models (one or several), while R^2 represents the variability explained by a given model. When a linear model is used, it is assumed that $R^2 = r_P^2$. However, this assumption may not be true in all cases. Furthermore, r_P calculated for variables AB is the same as that calculated for BA, but R^2 is exclusive of a particular model.

8. Pearson's coefficient measures the degree of linear association, while Spearman's simply measures the degree of association. Spearman's coefficient is more robust if all that is sought is the degree of association.

9. Statistical ranges are defined as hierarchical indicators of a data set. A value of 1 is assigned to the smallest number in the series, the next smallest number is labeled with 2 and so on. The maximum range is equal to the number of data points. In the case of data points with the same values, the mean of the ranges assigned to the repeated number is calculated and assigned.

10. It is the sum of the valid data points divided by the number of pixels contributing to the valid data.

11. In general, the mean is considered representative of the data set but for satellite data sets, the geometric mean is more representative than the arithmetic mean.

12. It is important that all the images have the same geographic projection because it facilitates writing a data extraction program based on data matrices of latitude, longitude and geophysical values. If the images did not have the same projection, the matrices would have different dimensions, which would require another entry variable in the data extraction process.

15.6 References

Barocio-León O, Millán-Núñez R, Santamaría-del-Ángel E, González-Silvera A (2007) Phytoplankton primary production in the euphotic zone of the California Current System from CZCS imagery and modeling. Ciencias Marinas 33(1): 59-72

Bograd SJ, Checkley DA, Wooster WS (2003) CalCOFI: a half century of physical, chemical, and biological research in the California Current System. Deep Sea Res II 50 (14-16): 2349-2353

Camacho-Ibar VF, Hernández-Ayón M, Santamaría-del-Ángel E, Dásele-Heuser LW, Zertuche-González JA (2007) Correlation of surges with carbon stocks in San Quintín Bay, a coastal lagoon in northwest Mexico. In: Hernández de la Torre B, Gaxiola Castro G (eds). Carbon in Aquatic Ecosystems of Mexico. Co-edited by the Department of Environmental and Natural Resources, National Ecology Institute NEI and the Center for Scientific Research and Higher Education of Ensenada CICESE, Mexico City pp 355-370

Cox PM, Betts RA, Jones CD, Spall SA, Totterdell IJ (2000) Acceleration of global warming due to carbon-cycle feedbacks in a coupled climate model. Nature 408, 184-187

Cullen, JJ, Eppley RW (1981) Chlorophyll maximum layers of the Southern California Bight and possible mechanisms of their formation and maintenance. Oceanol Acta 4: 23-32

Djavidnia S, Mélin F, Hoepffner N (2006) Analysis of Multi-Sensor Global and Regional Ocean Colour Products. MERSEA - IP Marine Environment and Security for the European Area - Integrated Project Report on Deliverable D.2.3.5 European Commission - Joint Research Centre Ref: MERSEA-WP02-JRC-STR-0001-01A.pdf. 228 pp

Dulvy N, Chassot E, Heymans J, Hyde K, Pauly D, Platt T, Sherman K (2009) Climate change, ecosystem variability and fisheries productivity. In: Forget M-H, Stuart V, Platt, T (eds), Remote Sensing in Fisheries and Aquaculture. IOCCG Report No. 8, IOCCG, Dartmouth, Canada pp 11-28

Di Lorenzo E, Miller AJ, Neilson DJ, Cornuelle BD, Moisan JR (2004) Modelling observed California Current mesoscale eddies and the ecosystem response. Int J Rem Sens 25(7-8): 1307 - 1312

Eber LE, Hewitt RP (1979) Conversion Algorithms for CALCOFI Station Grid. CalCOFI Rep XX: 135-137

Friedlingstein, P, Cox PM, Betts RA, Bopp L, Von Bloh W, Brovkin V et al (2006) Climate-carbon cycle feedback analysis: results from the C4MIP model intercomparison. J Climate 19(14): 3337-3353

Gregg WW, Casey NW (2004) Global and regional evaluation of the SeaWiFS chlorophyll data set. Rem Sens Environ 93: 463-479

González-Silvera AG, Santamaría-del-Ángel E, Millán-Núñez R, Manzo-Monrroy H (2004) Satellite observations of mesoscale eddies in the Gulfs of Tehuantepec and Papagayo (Eastern Tropical Pacific). Deep Sea Res II 51: 587-600

González-Silvera AG, Santamaría-del-Ángel E, Millán-Núñez R (2006) Spatial and temporal variability of the Brazil-Malvinas Confluence and the La Plata Plume as seen by SeaWiFS and AVHRR imagery. J Geophys Res 111: C06010, doi: 10.1029/2004JC002745

Haidvogel DB, Wilkin JL, Young RE (1991) A semi-spectral primitive equation ocean circulation model using vertical sigma and orthogonal curvilinear horizontal coordinates. J Comput Phys 94: 151-185

IOCCG (2000) Remote Sensing of Ocean Colour in Coastal, and Other Optically-Complex, Waters. Sathyendranath, S (ed), Reports of the International Ocean-Colour Coordinating Group, No. 3, IOCCG, Dartmouth, Canada

IOCCG (2004) Guide to the Creation and Use of Ocean-Colour, Level-3, Binned Data Products. Antoine, D (ed), Reports of the International Ocean-Colour Coordinating Group, No. 4, IOCCG, Dartmouth,

Canada
IOCCG (2006) Remote Sensing of Inherent Optical Properties: Fundamentals, Tests of Algorithms, and Applications. Lee, Z-P (ed), Reports of the International Ocean-Colour Coordinating Group, No. 5, IOCCG, Dartmouth, Canada
IOCCG (2007) Ocean-Colour Data Merging. Gregg W (ed), Reports of the International Ocean-Colour Coordinating Group, No. 6, IOCCG, Dartmouth, Canada
IOCCG (2009) Remote Sensing in Fisheries and Aquaculture. Forget M-H, Stuart V, Platt T (eds), Reports of the International Ocean-Colour Coordinating Group, No. 8, IOCCG, Dartmouth, Canada
Lewis MR (1992) Satellite ocean colour observations of global biogeochemical cycles. In: Falkwoski PG, Woodhead AD (eds). Primary Productivity and Biogeochemical Cycles in the Sea. Plenum Press NY pp 139-154
Lopez-Calderon J, Martinez A, Gonzalez-Silvera A, Santamaria-del-Angel E, Millan-Nuñez R (2008) Mesoscale eddies and wind variability in the northern Gulf of California. J Geophys Res 113: C10001, doi:101029/2007JC004630
Millán-Núñez R, Alvarez-Borrego S, Trees CC (1996) Relationship between deep chlorophyll and surface chlorophyll concentration in the California Current System. CalCOFI Rep 37: 241-250
Müller-Karger FE, Walsh JJ, Evans RH, Meyers MB (1991) On the seasonal phytoplankton concentration and sea surface temperature cycles of the Gulf of Mexico as determined by satellites, J Geophys Res 96(C7):12,645-12,665
OŔeilly JE, and 24 other authors (2000) Ocean colour chlorophyll-*a* algorithms for SeaWiFS, OC2, and OC4: version 4 In: Hooker SB, Firestone ER (eds) SeaWiFS Postlaunch Tech Rep Ser, Vol 11. SeaWiFS postlaunch calibration and validation analyses, Part 3. NASA, Goddard Space Flight Center, Greenbelt, MD, pp 9-23
Pelaez J, McGowan JA (1986) Phytoplankton pigment patterns in the California Current as determined by satellite. Limnol Oceanogr 31(5): 927-950
Platt T, Sathyendranath S, Caverhill CM, Lewis MR (1988) Oceanic primary production and available light: further algorithms for remote sensing. Deep-Sea Res 35: 855-879
Santamaría-del-Ángel E, Alvarez-Borrego S, Müller-Karger FE (1994a) Gulf of California biogeographic regions based on coastal zone color scanner imagery. J Geophy Res 99(C4): 7411-7421
Santamaría-del-Ángel E, Alvarez-Borrego S, MÃijller-Karger FE (1994b) The 1982-1984 El Niño in the Gulf of California as seen in coastal zone color scanner imagery. J Geophy Res 99(C4): 7423-7431
Santamaría-del-Ángel E, Millán-Núñez R, González-Silvera AG, Muller-Karger FE (2002) The color signature of the Ensenada Front and its seasonal and interannual variability. CalCoFi Rep 43: 156-161
Strub PT, Kosro PM, Huyer A, CTZ Collaborators (1991) The nature of the cold filaments in the California Current System. J Geophys Res 96(C8): 14,743-14,768
Traganza ED, Nestor DA, McDonald AK (1980) Satellite observations of nutrients upwelling off the coastal of California. J Geophys Res 85:4101-4106
Yoder JA, McClain CR, Blanton JO, Oey LY (1987) Spatial Scales in CZCS-Chlorophyll Imagery of the Southeastern U. S. Continental Shelf Limnol Oceanog 32(4): 929-941

15.6.1 Further reading

Rebstock GA (2003) Long-term change and stability in the California Current System: lessons from CalCOFI and other long-term data sets Deep Sea Res II 50(14-16): 2583-2594